Development of a new semi-mechanistic wall boiling heat transfer model for CFD methodology focusing on macroscopic parameters

Xiang Zhang [a], Xu Cheng [a,*], Wei Liu [b]

[a] *Institute for Applied Thermofluidics (IATF), Karlsruhe Institute of Technology (KIT), Kaiserstrasse 12, Karlsruhe 76131, Germany*
[b] *Department of Applied Quantum Physics & Nuclear Engineering, Kyushu University, 744 Motooka, Nishi-Ku, Fukuoka 819-0395, Japan*

ARTICLE INFO

ABSTRACT

Accurate prediction of flow boiling heat transfer is prominently dependent on the modeling of wall heat flux partitioning. In this paper, a new wall boiling heat transfer model was developed for three-dimensional Computational Fluid Dynamics (CFD) code to predict the wall heat flux and wall temperature. The proposed model partitioned the wall heat flux into convective heat flux and nucleate boiling heat flux, which were further modified by two correction factors. The key feature is that the new wall boiling heat transfer model was derived from bubble growth mechanism, incorporating reasonable assumptions, and each parameter within the model was calculated based on local physical properties and macroscopic parameters at the cell level. On this basis, the new wall boiling heat transfer model was coupled into ANSYS-Fluent and validated against various public experiments as well as the KIMOF experiments conducted under different conditions. Simulation results indicated that the proposed model could predict reasonable results for wall temperature and cross-section average void fraction. Finally, a comprehensive investigation was carried out to assess the sensitivity of the computational grids and the coefficients introduced in the new model.

1. Introduction

In comparison to liquid convection, flow boiling exhibits a more efficient heat transfer capacity owing to the latent heat associated with phase change and the enhancement effect by bubble disturbance. Therefore, flow boiling has received substantial attention in various industrial heat exchangers such as reactor, refrigeration, air-conditioning and applied to general energy conversion systems.

In the past few decades, numerous models for the calculation of wall heat flux have been developed, which could be broadly categorized into two categories: that predicting the overall wall heat flux by empirical correlations directly and that partitioning the total heat flux into various components based on the wall boiling heat transfer mechanism [1]. Empirical correlations are constructed by summarizing amounts of experimental data. In most of the empirical correlations, the wall heat flux is simply represented as a power function of the wall superheating temperature, with varying constant coefficients or indexes, such as the McAdams correlation [2]. Further, some empirical correlations incorporate physical parameters into the coefficients to account for pressure effects [3] and mass flux effects [4]. Fang et al. [5] and Mahmoud and Karayiannis [6] have conducted comprehensive reviews of empirical correlations for wall boiling heat transfer and assessed their calculating applicability to both water and R134a based on amounts of experimental database. Although these empirical correlations exhibit satisfactory performance within the respective range covered by the experiment data, their applicability is severely limited to particular operational conditions. It is challenging to assess the heat transfers with different boundaries and in different fluid channels by using a single empirical correlation. Therefore, empirical correlations for wall heat transfer are rarely employed in three-dimensional CFD software.

With the in-depth observation and comprehension of the boiling mechanism, several semi-mechanistic models have been proposed and employed to calculate wall heat flux boundary conditions in CFD. The semi-mechanism models attempt to describe the phenomenon of wall boiling heat transfer in detail by considering the specific physical processes involved in wall heat flux partitioning. The RPI model proposed by Kurul and Podowski [7] is a typical semi-mechanistic wall heat flux partitioning model, which was originally formulated for pool boiling. RPI model disaggregates the total wall heat flux into three terms, that are liquid convection term, evaporation term and quenching term, expressed as:

$$q_w = q_{fc} + q_q + q_e \tag{1}$$

Nomenclature

A_b	bubble cross section area /m^2	V	volume /m^3
A_i	phase interfacial area /m^2	w	bubble growth velocity /m·s^{-1}
$C_{p,l}$	specific heat capacity /J·kg^{-1}·K^{-1}		
D	diameter /m	*Greek letters*	
F_1	convective correction factor	α	void fraction
F_2	boiling correction factor	ρ	density /kg·m^{-3}
F_A	factor of vapor area effect	δ_T	thermal layer thickness /m
F_B	factor of boiling destructive effect	λ	thermal conductivity /W·m^{-1}·K^{-1}
h	heat transfer coefficient /W·m^{-2}·K^{-1}	σ	surface tension /N·m^{-1}
h_{fg}	latent of vaporization /J·kg^{-1}	μ	viscosity /kg·m^{-1}·s^{-1}
I	current /A		
L	length /m	*Subscripts*	
Pr	Prandtl number	e	evaporation
q	heat flux /W·m^{-2}	fc	liquid forced convection
Q	heat /W	i	inner
Q_L	heat loss /W	l	liquid
r	bubble radius /m	LB	superheated liquid to bubble
R_B	average bubble radius /m	nb	nucleate boiling
Re	Reynolds number	o	outer
T	temperature /K	P	pool boiling
T_b	bulk temperature in thermal layer /K	q	quenching
t	time /s	s	saturation
u_τ	shear velocity /m·s^{-1}	v / g	vapor
U	voltage/V	w	wall
		WL	wall to liquid
		WB	wall to bubble

Krepper et al. [8] studied the applicability of the RPI model in sub-cooled flow boiling calculations and demonstrated that the RPI model predicted the cross-sectional averaged void fraction in vertical tubes with good agreement to experimental data. In recent years, the RPI model has been widely accepted in various CFD codes for simulating wall boiling heat transfer processes [9]. Additionally, several researchers have contributed to improve the wall boiling heat transfer model based on RPI. Liu et al. [10] extended the RPI model by

introducing a vapor convection term and a transition function to predict boiling crisis. Shi et al. [11] modified the RPI model by dividing the quenching heat flux into two parts, including the sliding bubble and stationary bubble, to consider the effects of bubble sliding. Similarly, to evaluate the heat flux of sliding bubble within a narrow rectangular channel, Wang et al. [12] improved the RPI model by adding a sliding heat flux, which was calculated through transient heat flux integration.

However, as shown in Fig. 1, the more complex heat flux partition

q_w – wall heat flux
q_c – convection heat flux
q_e – evaporation heat flux
q_q – quenching heat flux
q_{ml} – micro-layer evaporation heat flux
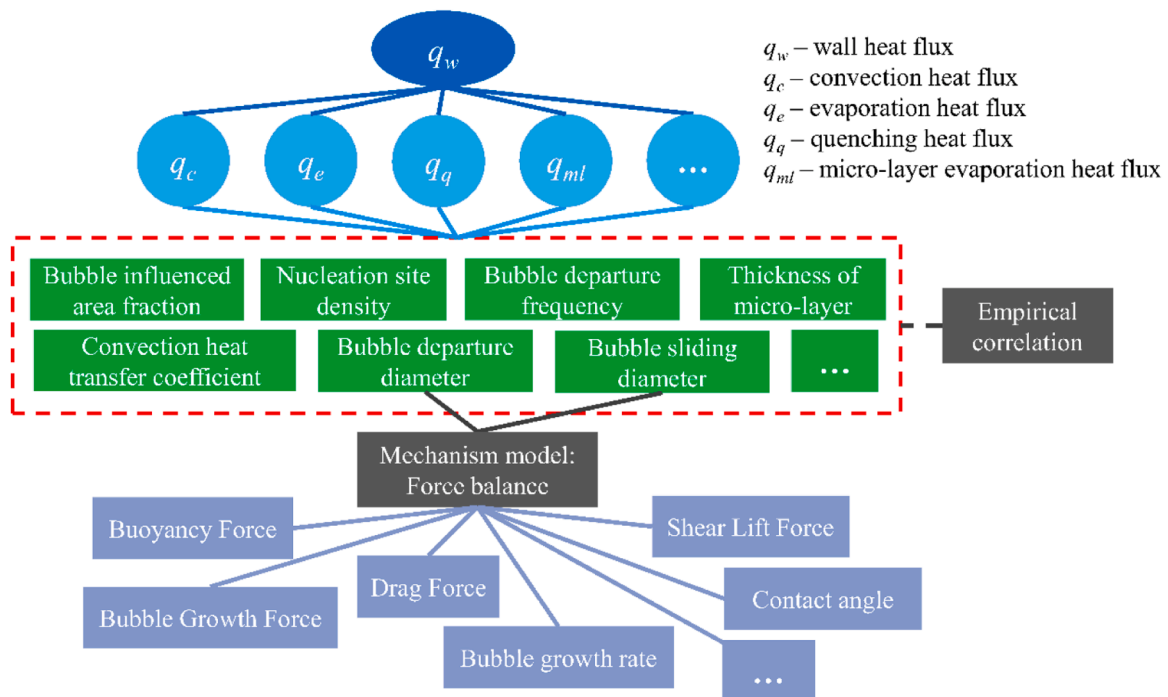
Fig. 1. Physical parameters in wall boiling heat transfer model based on RPI model.

means more microscopic parameters related to bubbles are needed to close the equations, such as the nucleation site density, bubble departure diameter, bubble sliding diameter, and so on. These microscopic parameters are usually calculated by using individual empirical correlations, as reviewed by Cheung et al. [13]. It is worth noting that the predictive capabilities of CFD approach are intrinsically reliant on the selection of the sub-models for these microscopic parameters and some specific coefficients used in empirical correlations. However, these sub-models are usually immature and condition limited, due to the large deviation in the experimental measurement of the microscopic parameters. Furthermore, a large number of different sub-models with different parameters can form different model combinations. Gu et al. [14] assessed the different performances of six combinations of the closure models, including nucleation site density, bubble departure diameter, and bubble departure frequency. Lin et al. [15] reviewed six distinct models for bubble departure diameter and seven models for bubble departure frequency, and combined them into 42 different combinations. They found that the different model combinations would give a large variation in results, and they concluded that there were no specific empirical correlations for the bubble departure diameter or bubble departure frequency that could always predict the results very well in different test conditions [15].

More recently, some mechanic models have been developed for calculating these microscopic bubble dynamic parameters, which seem involved detailed physical phenomena. Klausner et al. [16] developed a mechanic model for the bubble departure diameter and bubble lift-off diameter by the force balance analysis, which has been later evaluated and modified by other researchers [17]. However, as shown in Fig. 1, the adoption of the force balance mechanic model would require additional sub-models at the micro-level to describe the detailed physical parameters, thereby conferring augmented complexity upon the wall boiling heat transfer model and introducing more model uncertainties. Furthermore, it is important that the requirement of a large number of empirical correlations or mechanic sub-models within the wall boiling heat transfer model would present formidable challenges in terms of computational resources and iterative convergence in CFD simulations. For instance, it has been found that, by using the RPI model, it is difficult to obtain a convergency result under the working conditions with low pressure and low flow rate [18,19].

The Chen correlation [20] is also a well-known method for partitioning wall heat flux, frequently employed in engineering heat transfer analyses. It divides the total heat flux into two parts: the macroscopic heat transfer and microscopic heat transfer, expressing as:

$$q_w = F \cdot q_{mac} + S \cdot q_{mic} \tag{2}$$

The macroscopic heat transfer is presented by the forced convection mechanism, which is calculated using the Dittus-Boelter equation in the original Chen correlation [20]. An enhancement factor F for heat transfer is introduced to account for the disturbance effect caused by bubble motion. On the other hand, the microscopic heat transfer is established by the boiling mechanism and is corrected by a suppression factor S, to consider the thinner thermal boundary layer characteristic of subcooled flow boiling. Chen [20] empirically recommended values for the enhancement factor and suppression factor based on experimental best-fit curves related to the Martinelli number and effective two-phase Reynolds number. As summarized in Table 1, researchers have contributed in testing different empirical correlations for these two factors.

However, a challenge arises when applying the Chen correlation to three-dimensional CFD simulations, that is how to bridge the gap between the existing 1D correlations and the 3D-CFD model. For example, the Martinelli number and effective two-phase Reynold number are calculated based on bulk flow parameters that are not available in three-dimensional CFD simulations. It is quite difficult to define a reasonable bulk flow parameter and obtain a detailed hydraulic diameter for the CFD simulation in a complex flow channel. Additionally, the heat and

Table 1
Correlations of enhancement factor and suppression factor.

Refs.	Correlations
Kolev [21]	$F = \begin{cases} 2.35(1/X_{tt} + 0.213)^{0.736} & 1/X_{tt} > 0.1 \\ 1 & 1/X_{tt} \leq 0.1 \end{cases}$
Feldman et al. [22]	$F = 1 + 1.8(1/X_{tt})^{0.79}$
Qu and Mudawar [23]	$F = (1 + 1/X_{tt}^{0.5})^{1.78}$
Orian et al. [24]	$S = 1/[1 + 2.53 \times 10^{-6}(\mathrm{Re}_l F^{1.25})^{1.17}]$
Kolev [21]	$S = \begin{cases} 1/[1 + 0.12(\mathrm{Re}_{tp}^{1.14})] & \mathrm{Re}_{tp} < 32.5 \\ 1/[1 + 0.42(\mathrm{Re}_{tp}^{0.78})] & 32.5 \leq \mathrm{Re}_{tp} \leq 70 \\ 0.0797\exp(1 - \mathrm{Re}_{tp}/70) & \mathrm{Re}_{tp} > 70 \end{cases}$
Liu and Garimella [25]	$S = 0.9622 - 0.5822\arctan(\mathrm{Re}_l F^{1.25}/61800)$
Yan et al. [26]	$S = [T_{sat}/\Delta T_{sub}]/[1 + 2.53 \times 10^{-6}(\mathrm{Re}_l F^{1.25})^{1.17}]$

mass transfer in wall boiling is highly localized phenomenon, and relying solely on the two-phase Reynolds number may be insufficient to account for all the boiling mechanism effects, including the thermal boundary layer. Steiner et al. [27] attempted to localize the suppression factor by using the boiling departure lift-off (BDL) model. They divided the suppression factor into two components: one considering subcooling effects in the boundary layer and another considering flow effects based on the ratio of bubble departure diameter and lift-off diameter. Later, Sonntag [28] implemented and validated Steiner's model based on experiment data. Nevertheless, incorporating the force balance model into the BDL model for the suppression factor makes calculations more complex. Besides, the use of the bubble departure diameter-to-lift-off diameter ratio to represent flow effects may still need to be discussed in mechanism. Paz et al. [29] established the suppression factor relying on the Reynolds number. To obtain bulk properties, they proposed a search algorithm based on case geometry to identify the cell centroid within a given distance and assumed these cell properties as bulk properties. Das and Punekar [30] tried to re-evaluate the two-phase Reynolds number for CFD codes by a local Reynolds number, where velocity was taken as the dimensional velocity at y^+=250, and the hydraulic diameter was assumed as a constant value of 10 mm. The enhancement factor in the model of Das and Punekar was simplified to a ratio of heat transfer coefficient in liquid level and mixture level that calculated by Dittus–Boelter correlation. However, it is worth noting that, the value of the dimensional velocity and hydraulic diameter in the model of Das and Punekar are quite empirical and their applicability in different working conditions are still need to be validated. In an alternative view, Lin et al. [15] attempted to combine the Chen correlation with the RPI model. They used the RPI model to describe wall heat transfer processes but employed the Chen correlation to determine bubble departure frequency and replace the empirical model used in the RPI model. Nevertheless, amounts of physical parameters at micro level associated to bubble growth, such as the bubble departure diameter and nucleation site density, are yet needed to be evaluated.

From the review, it is shown that although the wall boiling heat transfer model in CFD methodology has been discussed by many researchers with different forms, there exists a pressing need for its further development, aiming to characterize the flow boiling mechanism by several heat flux terms while ensuring the independence of each partitioning from the bulk flow parameters. The model should be designed to yield a straightforward expression for heat flux partitioning and underpinned by mechanism foundation. In this study, a new semi-mechanistic wall boiling heat transfer model, employing heat flux partitioning methodology, is developed for three-dimensional CFD simulations. Different with the exiting RPI model that relies on microscopic bubble dynamic parameters, the new model focuses on local physical properties and macroscopic parameters at the cell level to enhance computational stability. To evaluate the performance of the new model, it will be implemented within ANSYS-Fluent through User-Defined-Function (UDF) and coupled with the Eulerian two-fluid framework to

simulate the flow boiling under different conditions. The calculation results will be validated by using various experimental data. Finally, sensitivity analysis of the grids and the coefficients within the proposed model will be performed.

2. Development of a new wall boiling heat transfer model

2.1. New wall boiling heat transfer model

As shown in Fig. 2, in the process of flow boiling, the heat from the heated wall is denoted be transferred by two mechanisms in this work:

(a) The heat transferred from the wall to the microlayer underneath bubble denotes as Q_{WB}, which will be used for bubble growth.
(b) The heat transferred from the wall to liquid directly denotes as Q_{WL}, which should be included in the liquid convection heat part.

Besides, Q_{LB} in Fig. 2 represents the heat transferred from the liquid thermal layer to the bubble. So that the total wall heat is expressed as:

$$Q_{total} = Q_{WL} + Q_{WB} \tag{3}$$

Based on the assumption that the heat transferred from the wall to the microlayer underneath bubble and used for bubble growth, in the subcooled flow boiling is equal to the same part of heat in the saturated pool boiling, that is $Q_{WB} = Q_{WB,P}$, the total wall heat can be rewritten as:

$$Q_{total} = Q_{WL} + Q_{WB,P} \tag{4}$$

Consequently, the new semi-mechanistic wall heat transfer model partitions the total wall heat flux into two parts, including the liquid convective part that transferred from the wall to liquid directly and the nucleate boiling part that be used for bubble growth with phase changing, as shown in Fig. 2:

$$q_w = F_1 \cdot q_{fc} + F_2 \cdot q_{nb} \tag{5}$$

where q_{fc} is the liquid convection heat flux, q_{nb} is the nucleate boiling heat flux, F_1 and F_2 are correction factors for the convection and boiling, respectively, that will be discussed in the following parts.

2.1.1. Liquid convective heat flux

The component of liquid convection heat flux is expressed as:

$$q_{fc} = h_{fc} \cdot (T_w - T_l) \tag{6}$$

in which, the liquid convection heat transfer coefficient is calculated by the wall function approach in Fluent [31], which has been a widely accepted methodology in CFD [15]:

$$T^* \equiv \frac{(T_w - T_p)\rho_l C_{p,l} C_\mu^{1/4} k_p^{1/2}}{q_{conv}} \tag{7}$$

$$T^* = \begin{cases} \Pr y^* & y^* < y_T^* \\ \Pr_t \left[\dfrac{1}{\kappa} \ln(E y^*) + P_J \right] & y^* > y_T^* \end{cases} \tag{8}$$

Fig. 2. Heat transfer during bubble growth.

$$y^* \equiv \frac{\rho_l C_\mu^{1/4} k_p^{1/2} y_p}{\mu_l} \tag{9}$$

where T^*, y^* and y_T^* are dimensionless temperature, wall distance and thermal sublayer thickness, T_p, k_p and y_p are temperature, turbulence kinetic energy and distance at the near wall node, respectively. And κ, C_μ, $\Pr_t$ and E are constants adopt as $\kappa = 0.4187$, $C_\mu = 0.09$, $\Pr_t = 0.85$ and $E = 9.793$. P_J is obtained by the empirical correlation recommended by Jayatillaka [32]. So that, the liquid convection coefficient is expressed as:

$$h_{fc} = \frac{\rho_l C_{p,l} C_\mu^{1/4} k_p^{1/2}}{T^*} \tag{10}$$

2.1.2. Convective correction factor

In wall boiling heat transfer, the efficiency of liquid convection will be changed under the influence of bubble dynamics. Thus, in this study, a convective correction factor F_1 need to be included to consider two effects caused by wall boiling heat transfer:

(a) In the process of wall boiling, a part of the heated surface will be covered by bubbles, which will not be taken into account for liquid convection heat transfer process.
(b) The liquid convective heat transfer will be enhanced due to the near wall thermal boundary layer is destroyed by the bubble growth in boiling process.

Thus, the convective correction factor is given as:

$$F_1 = F_A \cdot F_B \tag{11}$$

The bubble influenced area is defined as an area ratio effect. In this study, it is evaluated based on the local void fraction in the first-layer cell:

$$F_A = 1 - \alpha_g \tag{12}$$

The boiling effect is estimated by an enhancement factor F_B. In this study, it is expressed as a linear function of the ratio of the bubble growth velocity that contributed by evaporation to the shear velocity:

$$F_B = 1 + C_1 \frac{w}{u_\tau} = 1 + C_1 \frac{q_E}{h_{fg}\rho_v} \sqrt{\frac{\rho_l}{\tau_w}} \tag{13}$$

where C_1 is a coefficient, q_E represents the total evaporation heat flux for the bubble attached on the wall, which contains the heat flux from the heated wall and the heat flux translated through phase-interfaces in fluid.

2.1.3. Nucleate boiling heat flux

The nucleate boiling heat flux can be obtained by the Forster-Zuber model [33], which was also recommended in the Chen correlation [20] or other studies [34,35], expressing as:

$$q_{nb} = h_{nb} \cdot (T_w - T_s) \tag{14}$$

$$h_{nb} = 0.00122 \frac{\lambda_l^{0.79} C_{p,l}^{0.45} \rho_l^{0.49}}{\sigma^{0.5} \mu_l^{0.29} h_{lg}^{0.24} \rho_g^{0.24}} (T_w - T_s)^{0.24} (P_w - P_s)^{0.75} \tag{15}$$

2.1.4. Boiling correction factor

It is worth noting that the Forster-Zuber model [33] was derived for the total heat transfer in a saturated boiling. It means that the boiling heat flux obtained by the Forster-Zuber model contains both two parts of heat transfer that is $Q_{WL,P}$ and $Q_{WB,P}$, as denoted in Fig. 2. While, in the new wall boiling heat transfer model, the liquid convection part has been considered in the first term of Eq. (5) by the CFD wall function approach. So that the liquid convection part should be excluded from the boiling heat flux q_{nb} obtained by Forster-Zuber model. Consequently, a
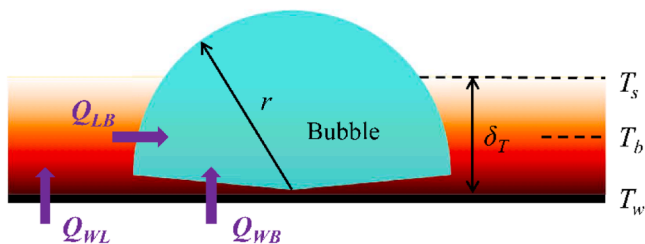
boiling correction factor F_2 is introduced to present the ratio of heat transfers:

$$F_2 = \frac{Q_{WB,P}}{Q_{WL,P} + Q_{WB,P}} = \frac{1}{1 + \frac{Q_{WL,P}}{Q_{WB,P}}} \tag{16}$$

Next, the most important thing is to derive the boiling correction factor F_2. Cooper [36] proposed a theory to calculate the growth rate of a bubble growing in liquid which is near to saturation temperature. Based on Cooper [36], the bubble growth rate can be approximately assumed to be two parts:

(a) Evaporation from the microlayer underneath bubbles:

$$r_{WB} = \frac{2}{C_2 \mathrm{Pr}_l^{0.5}} \frac{\rho_l C_{P,l}(T_w - T_s)}{\rho_v h_{fg}} a_l^{0.5} t^{0.5} \tag{17}$$

$$\frac{dr_{WB}}{dt} = \frac{1}{2}\left(\frac{2}{C_2 \mathrm{Pr}_l^{0.5}}\right) \frac{\rho_l C_{P,l}(T_w - T_s)}{\rho_v h_{fg}} a_l^{0.5} t^{-0.5} \tag{18}$$

(b) Evaporation from the sup-heated thermal layer at the interfacial curved surface:

$$r_{LB} = \left(\frac{12}{\pi}\right)^{0.5} \frac{\rho_l C_{P,l}(T_b - T_s)}{\rho_v h_{fg}} a_l^{0.5} t^{0.5} \tag{19}$$

$$\frac{dr_{LB}}{dt} = \frac{1}{2}\left(\frac{12}{\pi}\right)^{0.5} \frac{\rho_l C_{P,l}(T_b - T_s)}{\rho_v h_{fg}} a_l^{0.5} t^{-0.5} \tag{20}$$

The bulk temperature can be obtained by assuming a linear temperature distribution in liquid thermal boundary layer:

$$T_b = \frac{(T_w + T_s)}{2} \Rightarrow T_b - T_s = \frac{(T_w - T_s)}{2} \tag{21}$$

Recasting Eqs. (17) and (19) yield simplified forms:

$$r_{WB} = B_{WB} \cdot Ja \cdot a_l^{0.5} \cdot t^{0.5} \tag{22}$$

and

$$r_{LB} = B_{LB} \cdot Ja \cdot a_l^{0.5} \cdot t^{0.5} \tag{23}$$

where

$$B_{WB} = \frac{2}{0.8 \cdot \mathrm{Pr}_l^{0.5}} \tag{24}$$

$$B_{LB} = \frac{1}{2}\left(\frac{12}{\pi}\right)^{0.5} \tag{25}$$

$$Ja = \frac{\rho_l C_{P,l}(T_w - T_s)}{\rho_v h_{fg}} \tag{26}$$

$$a_l = \frac{\lambda_l}{\rho_l C_{P,l}} \tag{27}$$

Consequently, the two parts of bubble growth equations can be unified into:

$$r = B \cdot Ja \cdot a_l^{0.5} \cdot t^{0.5} \tag{28}$$

$$\frac{dr}{dt} = \frac{1}{2} B \cdot Ja \cdot a_l^{0.5} \cdot t^{-0.5} \tag{29}$$

The cross-section area of a bubble is given by:

$$A_b = \pi r^2 = \pi B^2 \cdot Ja^2 \cdot a_l \cdot t \tag{30}$$

From $t = 0$ to $t = \tau$, the time-averaged values of cross-section area and bubble radius are given by:

$$A_{b,ave} = \frac{\int_0^\tau A_b dt}{\tau} \tag{31}$$

$$R = \frac{\int_0^\tau r dt}{\tau} \tag{32}$$

Substituting Eqs. (28) and (30) into Eqs. (31) and (32) yields:

$$A_{b,ave} = \frac{\pi}{2} B^2 \cdot Ja^2 \cdot a_l \cdot \tau \tag{33}$$

$$R = \frac{1}{\sqrt{2}} B \cdot Ja \cdot a_l^{0.5} \cdot \tau^{0.5} \tag{34}$$

Based on the hemispherical assumption for the bubbles attached on the heated wall, the total heat transfer rate for evaporation is given by:

$$Q = \rho_v h_{fg} \frac{dV}{dt} = \rho_v h_{fg} 2\pi r^2 \frac{dr}{dt} \tag{35}$$

As shown in Fig. 2, the heat flux transferred through the two-phase interfacial surface is considered by two parts:

(1) The interfacial surfaces between the bubble and microlayer:

$$q_{WB} = \frac{Q_{WB,P}}{A_{i,WB}} \tag{36}$$

(2) The interfacial surfaces between the bubble and superheated thermal layer:

$$q_{LB} = \frac{Q_{LB,P}}{A_{i,LB}} \tag{37}$$

Substituting Eq. (35) into Eqs. (36) and (37) yields:

$$q_{WB} = \frac{\rho_v h_{fg} 2\pi r_{WB}^2}{\pi r_{WB}^2} \frac{dr_{WB}}{dt} = \rho_v h_{fg} B_{WB} \cdot Ja \cdot a_l^{0.5} \cdot t^{-0.5} \tag{38}$$

and

$$q_{LB} = \frac{\rho_v h_{fg} 2\pi r_{LB}^2}{2\pi r_{LB}^2} \frac{dr_{LB}}{dt} = \frac{1}{2}\rho_v h_{fg} B_{LB} \cdot Ja \cdot a_l^{0.5} \cdot t^{-0.5} \tag{39}$$

Finally, the effective heat transfer coefficients at any time point are given by:

$$h_{WB,eff} = \frac{q_{WB}}{T_w - T_s} \tag{40}$$

$$h_{LB,eff} = \frac{q_{LB}}{T_b - T_s} \tag{41}$$

Substituting Eqs. (21), (38) and (39) into Eqs. (40) and (41) yields:

$$h_{WB,eff} = \rho_v h_{fg} B_{WB} \cdot Ja \cdot a_l^{0.5} \cdot \tau^{-0.5} \Delta T^{-1} \tag{42}$$

$$h_{LB,eff} = \rho_v h_{fg} B_{LB} \cdot Ja \cdot a_l^{0.5} \cdot \tau^{-0.5} \Delta T^{-1} \tag{43}$$

Under the combined effects of the two mechanisms for bubble growth, we can express the actual radius for a hemispherical bubble in the unified form as given in Eq. (28):

$$r_B = B_B \cdot Ja \cdot a_l^{0.5} \cdot t^{0.5} \tag{44}$$

Thus, the averaged bubble radius from $t = 0$ to $t = t$ due to the combined effects of the two mechanisms is:

$$R_B = \frac{1}{\sqrt{2}} B_B \cdot Ja \cdot a_l^{0.5} \cdot \tau^{0.5} \tag{45}$$

As shown in Fig. 2, the heat conduction transferred from the wall to the liquid thermal layer is given as:

$$Q_{WL,P} = (1 - \alpha_g)\pi R_B^2 \cdot \lambda_l \frac{(T_w - T_s)}{\delta_T} \tag{46}$$

While the heat transferred from the liquid thermal layer to the bubble is calculated under the assumption of linear temperature distribution in the superheated layer and given as:

$$Q_{LB,P} = \alpha_g \cdot C_T 2\pi R_B \cdot \delta_T \cdot h_{LB,eff}(T_b - T_s) \tag{47}$$

where C_T is a coefficient considering the deviation introduced by simplifications, such as the linear distribution of temperature in the superheated thermal boundary layer and the bubble surface in superheated thermal boundary layer is simplified as a cylindrical shape, as shown in Fig. 3.

In saturated pool boiling, an assumption has been made that all the heat transferred from the wall to the liquid thermal layer is then transferred to the bubble through the interfacial surfaces between the bubble and superheated thermal layer, that is:

$$Q_{WL,P} = Q_{LB,P} \tag{48}$$

Substituting Eqs. (46) and (47) into Eq. (48) yields:

$$(1 - \alpha_g) \cdot \pi R_B^2 \cdot \lambda_l \frac{\Delta T}{\delta_T} = \alpha_g \cdot C_T 2\pi R_B \cdot \delta_T \cdot h_{LB,eff}(T_b - T_s) \tag{49}$$

The thickness of superheated thermal layer can be obtained from Eq. (49):

$$\delta_T = \left(\frac{1 - \alpha_g}{\alpha_g}\right)^{0.5} \cdot \left(\frac{R_B \cdot \lambda_l}{C_T h_{LB,eff}}\right)^{0.5} \tag{50}$$

Besides, the wall heat transferred through the microlayer to the vapor in an attached bubble can be expressed as:

$$Q_{WB,P} = \alpha_g \cdot \pi \cdot R_B^2 \cdot h_{WB,eff} \cdot (T_w - T_s) \tag{51}$$

From the Eqs. (47) and (51), we have:

$$\frac{Q_{WL,P}}{Q_{WB,P}} = \left(\frac{1 - \alpha_g}{\alpha_g}\right)^{0.5} \cdot C_T^{0.5} \cdot \lambda_l^{0.5} \cdot \frac{1}{R_B^{0.5}} \frac{h_{LB,eff}^{0.5}}{h_{WB,eff}} \tag{52}$$

Substituting Eqs.(40) and (41) into Eq.(52) yields:

$$\frac{Q_{WL,P}}{Q_{WB,P}} = \left(\frac{1 - \alpha_g}{\alpha_g}\right)^{0.5} \cdot C_T^{0.5} \cdot \frac{B_{LB}^{0.5}}{B_{WB}} \left(\frac{\lambda_l \cdot (T_w - T_s)}{\rho_v h_{fg} a_l^{0.5} Ja}\right)^{0.5} \left(\frac{\tau^{0.5}}{R_B}\right)^{0.5} \tag{53}$$

Assuming that the actual bubble volume has a linear relation with the volume contributed by the microlayer evaporation. So that, the actual bubble radius can be expressed by R_{WB}:

$$R_B = C_G \cdot R_{WB} = \frac{1}{\sqrt{2}} C_G \cdot B_{WB} \cdot Ja \cdot a_l^{0.5} \cdot \tau^{0.5} \tag{54}$$
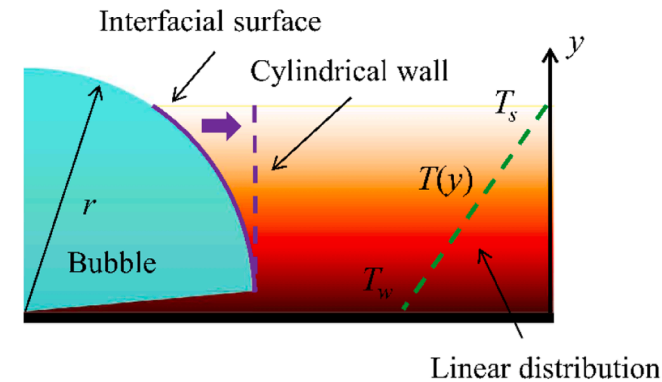
Fig. 3. Simplifications in the calculation of $Q_{LB,P}$.

Substituting Eqs. (54), (26) and (27) into Eq. (53) yields:

$$\frac{Q_{WL,P}}{Q_{WB,P}} = \left(\sqrt{2} \cdot \frac{1 - \alpha_g}{\alpha_g} \cdot \frac{C_T}{C_G} \cdot \frac{B_{LB}}{B_{WB}^2 \cdot B_{WB}} \cdot \frac{\rho_v h_{fg}}{\rho_l C_{P,l}}\right)^{0.5} \cdot \left(\frac{1}{T_w - T_s}\right)^{0.5} \tag{55}$$

Simplifying the ratio of two coefficients with one value, as:

$$C_2 = \frac{C_T}{C_G} \tag{56}$$

Finally, we can obtain the correlation of boiling correction factor based on local macroscopic parameters by substituting Eqs. (55) and (56) into Eq. (16), that is:

$$F_2 = \frac{1}{1 + \left(\sqrt{2} \cdot C_2 \cdot \frac{1 - \alpha_g}{\alpha_g} \cdot \frac{B_{LB}}{B_{WB}^2 \cdot B_{WB}} \cdot \frac{\rho_v h_{fg}}{\rho_l C_{P,l}}\right)^{0.5} \cdot \left(\frac{1}{T_w - T_s}\right)^{0.5}} \tag{57}$$

where B_{WB} and B_{LB} are coefficients for bubble growth, the empirical correlations Eqs. (24) and (25) recommended by Cooper [36] are employed in this study.

2.2. Summary of the new model

In the preceding section, a new wall boiling heat transfer model has been developed based on the partitioning mechanism. The characteristic of the new model is that its ultimate correlation primarily centers on macroscopic variables, such as physical properties, temperature, and void fraction. It is a completely three-dimensional model, predicated on local cell-level parameters, and is independent of the parameters in bulk flow, such as bulk velocity or hydraulic diameter. Furthermore, the new model obviates the necessity for all micro-parameters, such as nucleation site density and bubble behaviors, which are requisite components of the existing partitioning models, such as the widely applied RPI model.

2.2.1. Basic assumptions

In order to establish the new wall boiling heat transfer model, several simplifying assumptions have been introduced during derivation. The primary assumptions are summarized as following:

(1) In subcooled flow boiling, it is assumed that the heat transferred from the wall to the microlayer underneath the vapor bubble, using for bubble growth, is equivalent to the corresponding part of heat observed in saturated pool boiling. It is expressed as $Q_{WB} = Q_{WB,P}$.

(2) In case of saturated pool boiling, all the heat transferred from the wall to the liquid thermal boundary layer is assumed to be totally transferred to the bubble through the interfacial surfaces between the bubble and the superheated thermal layer. It is expressed as $Q_{WL,P} = Q_{LB,P}$.

(3) The process of bubble growth is assumed to be thermal-controlled.

(4) The temperature distribution within the liquid thermal boundary layer is assumed to follow a linear profile along the normal distance from the wall.

(5) The morphology of the growing vapor bubbles, which are attached on the heated wall, are assumed to be hemispherical.

2.2.2. Discussion on the coefficients

The new wall boiling heat transfer model introduced two coefficients in the final correlation. The first coefficient C_1 is appeared in the convection enhancement factor correlation, as given in Eq. (13) and serves as a metric for quantifying the destructive effect of bubble growth on the superheated thermal layer, which will enhance the convective heat transfer. In the following sections, we will adopt a value of 10 for C_1 to preliminarily validate the performance of model.

The second coefficient C_2 is a combination of C_T and C_G, as shown in

Eq. (56). The C_T, introduced in Eq. (47), is used to correct the calculation of heat transferred from the superheated thermal layer to the bubble. This correction is necessitated due to the assumption of a linear temperature distribution and the simplification of two-phase interfacial transfer area. Considering this, it is estimated that the value of C_T should be around 1. On the other hand, the coefficient C_G is introduced in Eq. (54) to accommodate the simplification of the linear relationship between the actual bubble volume and the volume contributed by microlayer evaporation. Various researchers have studied the evolution of the microlayer and its contribution to overall bubble growth. For example, Demiray and Kim [37] reported that approximately 12.5 % of the energy required for bubble growth was derived from the microlayer, while Jung and Kim [38] proposed that the heat transfer through the microlayer constituted less than 17 % of the total. Utaka et al. [39] elucidated the heat transfer characteristics in nucleate pool boiling for both water and ethanol, with a specific focus on microlayer structure. They discovered that the percentage contributions to the total bubble volume through microlayer evaporation ranged from 15 % to 70 % within the surface superheat range at bubble inception of 6–39 K. Consequently, by combining the functions of C_T and C_G, the reference value 0.7 for C_2 is employed in the subsequent validating simulations.

The sensitivity analysis of these two coefficients will be further discussed in Section 4 within an estimated range.

3. Validation of the new model

In order to assess the performance of the new wall boiling heat transfer model, different experiments are simulated. The calculated results are compared with the experimental data.

3.1. Numerical configuration and solver in Fluent

To simulate a flow boiling case, the Eulerian two-fluid framework is employed, which solves the governing equations for two-phases, respectively. The new wall boiling heat transfer model is recompiled with the two-fluid framework in ANSYS-Fluent as an external code by User Defined Function (UDF) to calculate the heat flux partitioning, temperature and interfacial mass transfer at the heated wall. The interfacial transfers, including mass, momentum, and energy, are obtained by sub-models and incorporated as source terms. The auxiliary models, employed in this study to close the governing equations, are summarized in Table 2. Fig. 4 shows the solving sequence of the developed wall boiling heat transfer model within the two-fluid framework. For each identified first-layer grid near the heated wall, the new wall boiling heat transfer model is solved in each iteration, as indicated by the red block in Fig. 4. Since the non-linear relationship between the wall heat flux and wall temperature, an inner-iteration process is necessary within the given boundary conditions of total heating power. In this study, the wall heat flux partition and correction factors will be calculated based on an initial assumed wall temperature at first. The

Table 2
Auxiliary models to close the equations.

Physical parameter	Model/Correlation
Wall boiling heat transfer	New wall boiling heat transfer model
Turbulence	Standard k-ε model [40]
Turbulence interaction	Sato model [41]
Interfacial transfers	
Interfacial area concentration	Symmetric model [31]
Bubble diameter	Improved Unal model [31]
Drag force	Ishii model [42]
Lift force	Moraga model [43]
Wall lubrication force	None
Turbulent dispersion force	Lopez-de-Bertodano model [44]
Liquid-interface heat transfer	Ranz-Marshall model [45]
Vapor-interface heat transfer	Lavieille et al. model [46]
Interfacial mass transfer	Energy balance [31]

calculated heat flux and the given boundary will be used to judgement the calculation convergence. The method of bisection is implemented for estimating wall temperature to help to accelerate convergence.

3.2. Validation with reference experiments

3.2.1. Bartolemei experiment [47]

Bartolemei and Chanturiya [47] conducted a subcooled flow boiling experiment in a vertical pipe, which has been widely implemented for validating CFD models. The working fluid was water. The test tube had a length of 2 m with uniform heating power and a diameter of 15.4 mm. Table 3 provides an overview of the boundary conditions. The mesh4 given in Table 6 will be implemented in this part, while the effects of different mesh sizes will be discussed in Section 4.1 in detail. As shown in Fig. 5, the predicted wall temperature agrees with the measurement data very well. The wall temperature is increased at the beginning of channel as the continuous heat input, but a little decreased at the height around 0.8 m. This is because that the heat transfer coefficient is initially dominated by single-phase convection mechanism, while with the increase of wall superheat, the heat transfer coefficient is enhanced under the effect of boiling. However, it can be seen that the RPI model under-predicts wall temperature in this specific region. In the downstream area of the channel, the wall temperature increases slightly in both current model and RPI model, due to the efficient heat transfer in subcooled flow boiling. The cross-section average liquid temperature is consistence with the experiment data. However, an over-prediction of average void fraction is observed near the pipe exit, although the position where the average void fraction appears is reasonably captured. The larger cross-section average void fraction may not only be resulted by the wall boiling heat transfer model, but also could be a result of the deviation in the interfacial transfers within the bulk flow. In general, the results evident that the new wall boiling heat transfer model simulates the Bartolemei experiment with a satisfactory accuracy.

Fig. 6 illustrates the partitioning of wall heat flux and the associated correction factors calculated by the new model. As the wall temperature exceeds saturation temperature, a noteworthy transition occurs in the heat transfer mechanism. Specifically, the liquid convection heat flux begins to reduce while the boiling heat flux begins to play a more significant role. However, as depicted in Fig. 6(b), since the boiling destructive effect of the liquid thermal-layer is enhanced with the escalating production of bubbles, a brief increasement of the liquid convection heat flux is observed at an approximate height of 0.7 m. Eventually, the boiling heat transfer dominates due to its high efficiency. An additional observation pertains to the void fraction within the first-layer grid downstream of the test section (at a height of $H = 1.6$ m) with a high quality. Here, the void fraction declines due to more bubbles gradually move towards the central region of the pipe. This migration is driven by phase interaction forces, such as lift force and turbulent dispersion force, as presented in Fig. 7(a) showcasing the radial distribution of void fraction at different heights. This reduction in void fraction within the first-layer grid leads to a temporary increase in liquid convection heat flux. This phenomenon arises because, in the high-quality region, the presence of bubbles on the wall decreases, simultaneously reducing the bubble influenced area. This, in turn, results in an increase in the convective correction factor, as outlined in Eqs. (11) and (12). Nevertheless, as corroborated by Fig. 7(b), the liquid temperature near the heating wall reaches the saturation temperature, which means that there is no condensation heat transfer between the bubble and the liquid in the first-layer, while vapor production in the first-layer comes from two sources: evaporation occurring on the heated wall and evaporation from phase interfaces. So that the void fraction in the first-layer commences an upward trend after reaching a height of 1.8 m.

3.2.2. DEBORA experiment [48]

Three cases under different working conditions, as listed in Table 4, are selected from the DEBORA experiments [48] to assess the new model
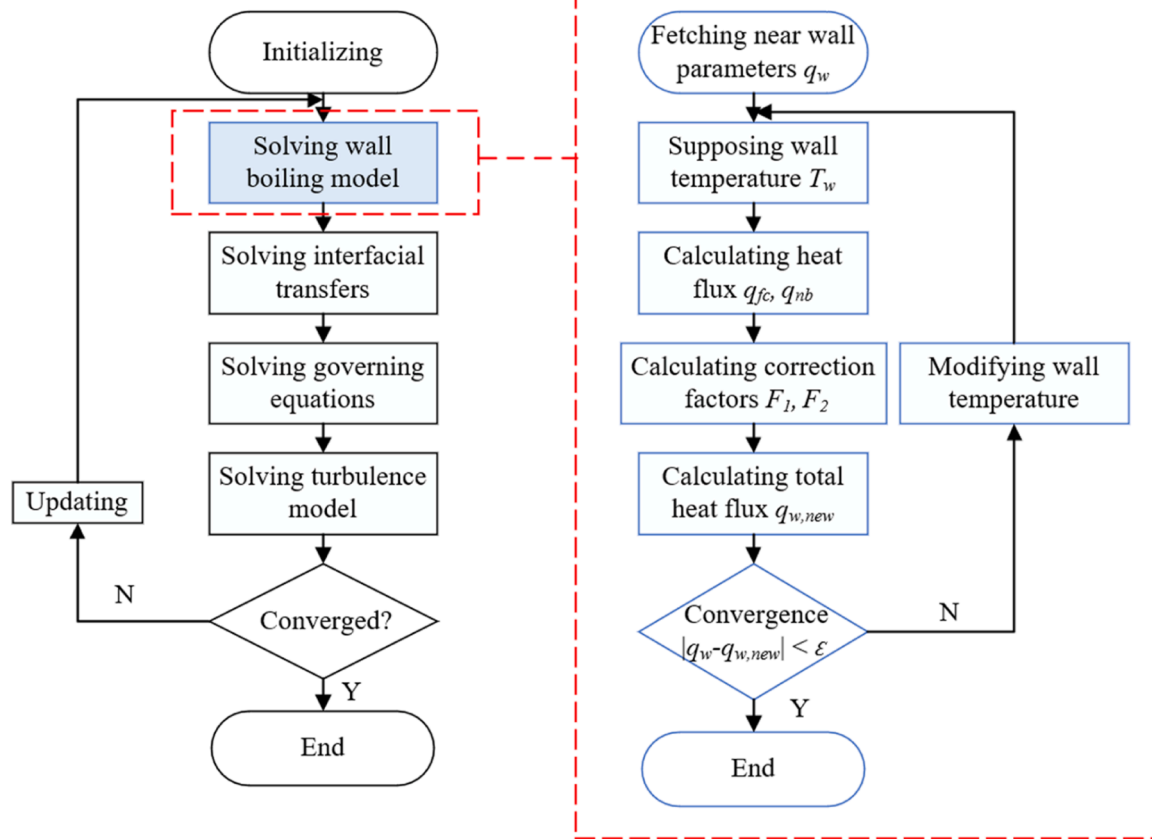
Fig. 4. Solving sequence of models.

Table 3
Boundary conditions of Bartolemei experiment.

No.	Pressure (MPa)	Mass flow rate (kg/m²/s)	Heat flux (W/m²)	Subcooled temperature (K)
Bar	4.5	900	570,000	58.2
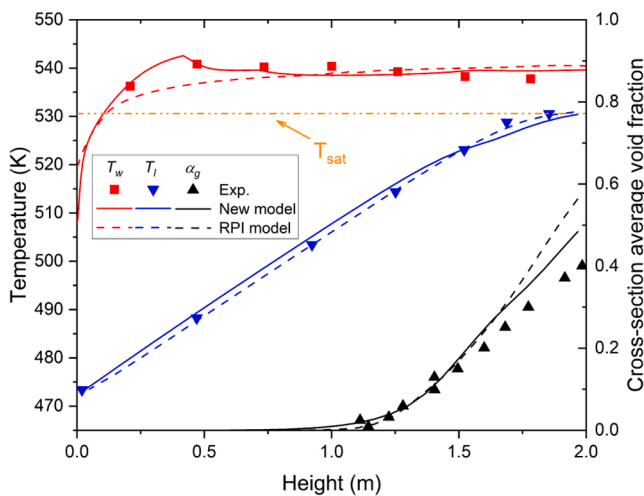
Fig. 5. The calculated results of Bartolemei experiment.

in this part. The DEBORA experiment is conducted within vertical pipes possessing a diameter of 19.2 mm, with an axial heating length of 3.5 m. The dataset comprises valuable measurements, encompassing wall temperature, average void fraction, and liquid temperature at the exit. It is worth noting that the working fluid is refrigerant R-12, exhibiting a density ratio of approximately 5.9 under 2.62 MPa, a value similar to the density ratio of water under 15.7 MPa, which is 5.7. A structural mesh comprising 50 uniformly distributed nodes in the radial direction and 1500 uniformly distributed nodes in the axial direction is utilized. The radial grid has been meticulously refined as much as possible but control the wall Y-plus exceeds a value of 30, as mandated by the specifications of the standard k-ε turbulence model and wall function. In Fig. 8, the comparative results are illustrated. Notably, the wall superheat temperature is overestimated, signifying that the new wall boiling heat transfer model underestimates the heat transfer coefficient within these cases.

3.3. Validation with KIMOF experiment

3.3.1. Experimental facility

In order to study the thermal-hydraulic characteristic of flow boiling and boiling crisis, the KIT Model Fluid Facility (KIMOF) has been built at the Karlsruhe Institute of Technology. The test loop of KIMOF is shown in Fig. 9. After leaving the pump, the Refrigerant R-134a, which was used as the working fluid, would be pre-heated by the preheater and flow through the vertically installed test pipe. The fluid be cooled after leaving the test section by two independent cooling systems. The operating pressure was regulated by a pressurizer that used hydraulic oil on the second side. The fluid flow rate was measured by a Coriolis mass flow meter before entering the test section. In total, 55 T-type thermocouples were arranged along the test pipe to monitor the outside wall temperature. A more detailed description of KIMOF can be found in the Ref. [49].

The test pipe was covered with thermal insulation material to minimize the heat loss to the environment. As given in the Ref. [49], the
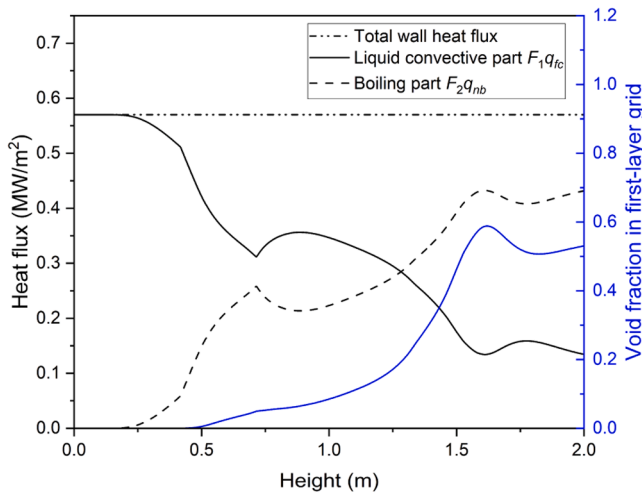
(a) Wall heat flux partitioning
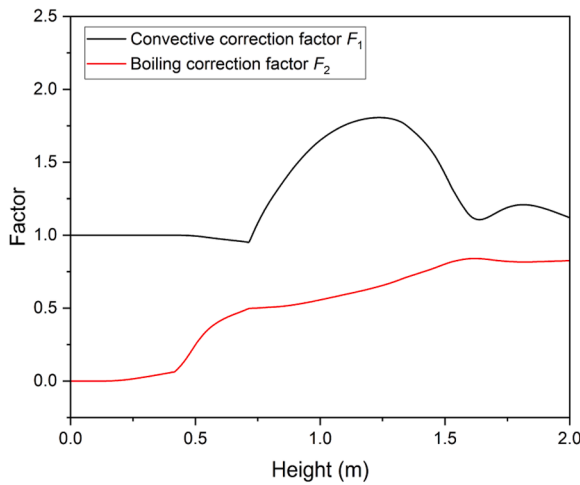
(b) Correction factors

Fig. 6. Axial parameters.

(a) Void fraction

(b) Liquid temperature

Fig. 7. Radial parameters.

wall heat flux is calculated by:

$$q_w = \frac{UI - Q_L}{\pi L D_i} \tag{58}$$

The inner wall temperature is obtained by:

$$T_{w,i} = T_{w,o} - \left(\frac{q_V}{16\lambda}\right)\left(D_i^2 - D_o^2\right) + \frac{D_o}{2\lambda}\left[\left(\frac{q_V D_o}{4} - q_L\right)\log\left(\frac{D_i}{D_o}\right)\right] \tag{59}$$

where q_V is the volumetric heat flux, q_L is the heat loss at outer wall and was determined using the calibration experiments. The measurement device uncertainties of temperature, mass flux, and pressure are provided by the manufacturers as ±0.5 °C, ±0.05 %, and ±0.25 %, respectively.

3.3.2. Simulation cases

In this investigation, three pressure conditions have been chosen. All the test conditions are shown in Table 5. The fluid flows through a circular channel with a length of 3 m and a diameter of 0.01 m. Uniform heating power is applied to all experiments conducted within KIMOF. As in prior simulations, the mesh utilized in this section has been meticulously refined to its maximum extent in the radial direction, but at the same time ensure that the wall Y-plus exceeds a value of 30, in

accordance with the stipulations of the standard *k-ε* turbulence model and wall function. Finally, to conduct KIMOF simulations, a structural mesh is adopted, consisting of 20 equidistant nodes distributed radially and 2000 equidistant nodes distributed axially. The velocity-inlet boundary and pressure-outlet boundary are employed for simulations.

3.3.3. Comparison of simulation results and experimental data

The comparative analysis between the simulation data generated using the new wall boiling heat transfer model and experimental data

Table 4
Boundary conditions of DEBORA experiment.

No.	Pressure (MPa)	Mass flow rate (kg/m²/s)	Heat flux (W/ m²)	Subcooled temperature (K)
DEB1	2.62	1996	73,890	18.31
DEB2	2.62	1985	73,890	16.3
DEB3	1.46	2030	76,240	26.94
DEB4	1.46	2024	76,260	13.89
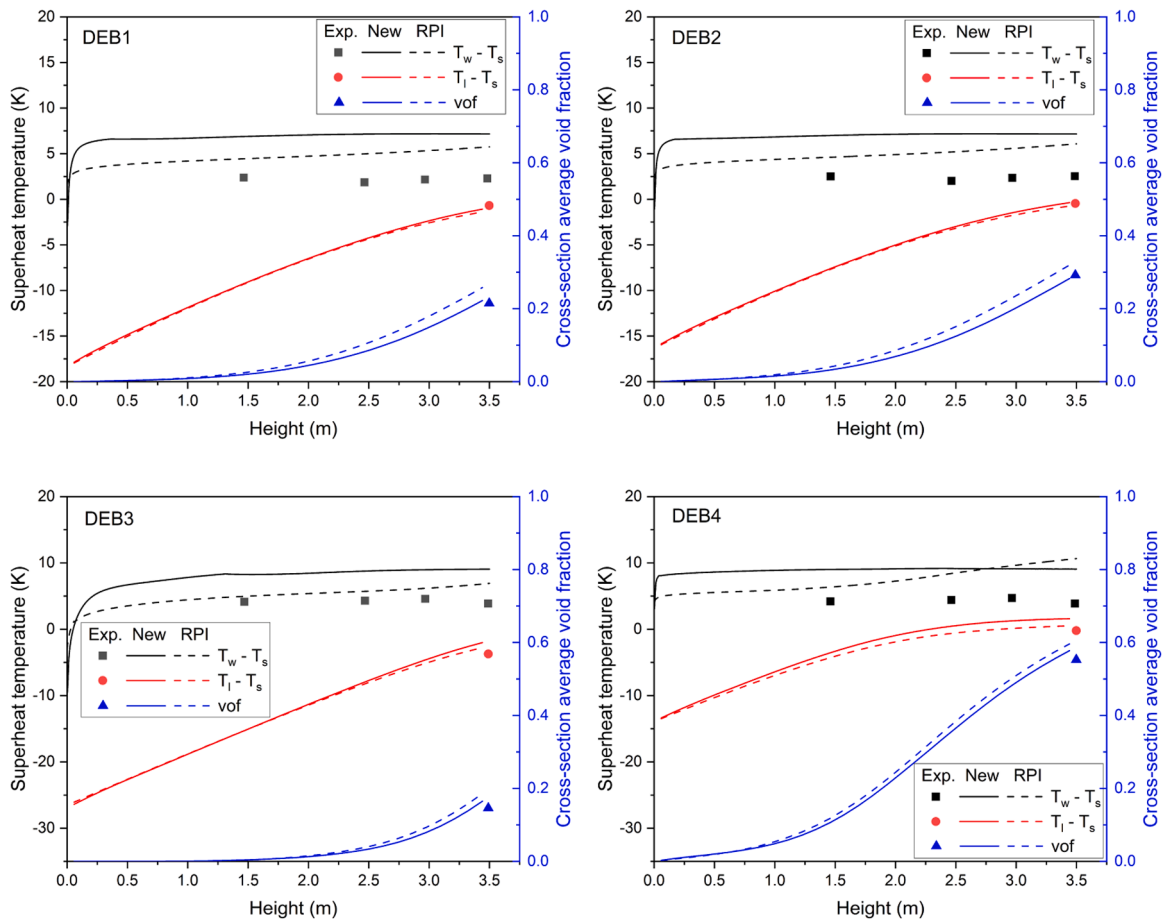
Fig. 8. The calculated results of DEBORA experiment.
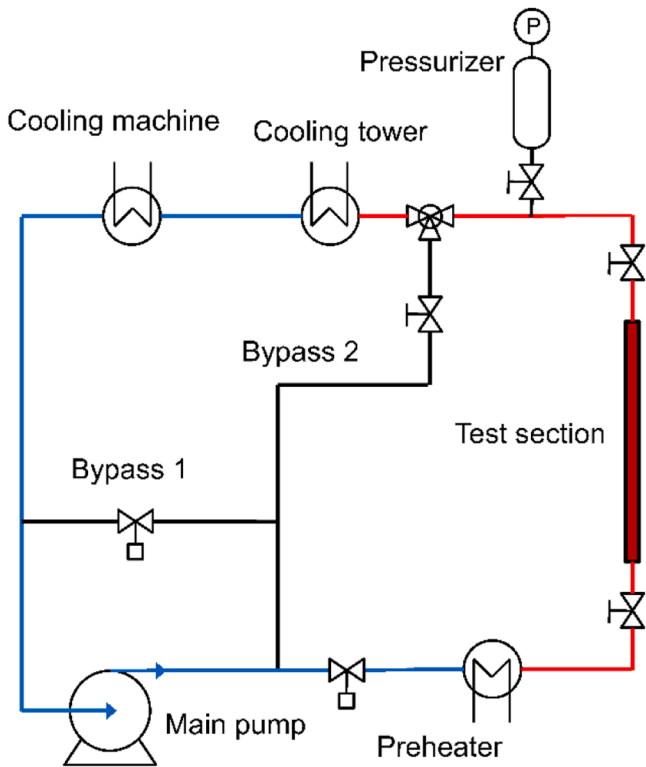
Fig. 9. Experiment loop of KIMOF facility [49].

Table 5
Boundary conditions of IATF experiment.

No.	Pressure (MPa)	Mass flow rate (kg/m²/s)	Heat flux (W/ m²)	Subcooled temperature (K)
IATF1	2.84	600	51,500	44.58
IATF2	2.84	600	42,000	25.58
IATF3	2.84	600	30,000	5.58
IATF4	2.84	1500	44,500	4.58
IATF5	2.84	1500	119,000	54.58
IATF6	1.1	1482.61	79,822.3	4.87
IATF7	1.1	1101.89	75,009.9	10.28
IATF8	1.1	1296.97	79,901.2	10.19
IATF9	1.1	1501.41	84,763.3	10.23
IATF10	1.1	298.275	39,868.7	10.28
IATF11	1.1	498.059	55,033.4	10.6
IATF12	1.1	689.893	65,115.9	10.21
IATF13	1.1	897.832	70,202	10.16
IATF14	1.6	1497.92	60,296.8	5.03
IATF15	1.6	302.114	30,076.5	10.89
IATF16	1.6	494.994	40,001	10.96
IATF17	1.6	691.951	45,026.6	10.41
IATF18	1.6	897.66	50,240.8	10.71
IATF19	1.6	1098.93	59,744.6	10.75
IATF20	1.6	1301.03	65,175	10.24
IATF21	1.6	1495.18	69,948	10.99

conducted under 2.84 MPa is presented in Fig. 10. The results showed that the new model produces under-prediction in case IATF1, IATF2 and IATF5. It can be seen that, in case IATF1, IATF2 and IATF5, the wall temperature rapidly increases at the entrance of test section, primarily due to the increasement of liquid temperature. In contrast, cases IATF3 and IATF4 start with high wall temperature and exhibit only a marginal

(a) IATF1 - IATF3

(b) IATF4 - IATF5
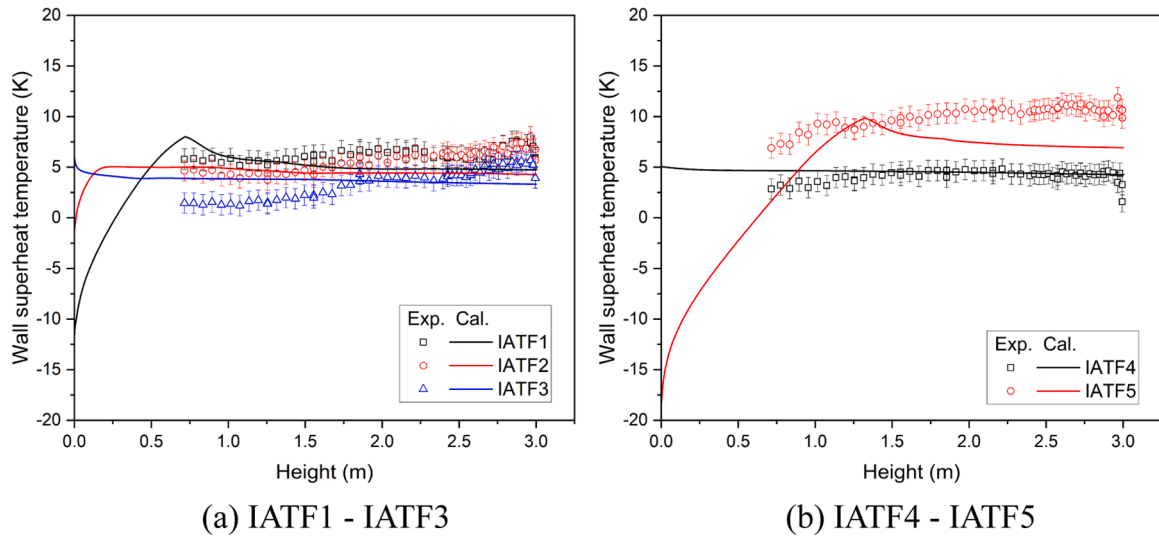
Fig. 10. Results of IATF experiments at 2.84 MPa.

change in wall temperature, attributed to its lower inlet subcooling conditions. As the decreasing of liquid superheat near the heating wall, the rate of wall temperature increment gradually decelerates and, in some cases, even experiences slight declines. This phenomenon can be attributed to the engagement of subcooled flow boiling mechanism in the wall heat transfer process, thereby enhancing overall heat transfer efficiency. However, it is important to note that in some conditions, such as in case IATF1, the identification of the peak of wall temperature may be slightly delayed, suggesting potential areas for further refinement of the correct factors established in this study. Finally, the wall temperature becomes stabilized that is consistent with the experimental observations.

Figs. 11 and 12 presents the comparison results at 1.1 MPa and 1.6 MPa, respectively. It is evident that the measured wall temperature is overestimated in all cases, with an associated deviation range of approximately 2–3 K, thereby indicating an under-prediction of the heat transfer coefficient. Given the low inlet subcooling prevalent in these cases, the dominance of the boiling heat transfer mechanism is observed throughout most sections of the tube. Consequently, it is plausible that the deviation is due to the calculation of the boiling heat transfer coefficient, which is based on the Forster-Zuber model [33] in this study,

may need to be improved for the fluid of refrigerant R134a under 1.1 MPa and 1.6 MPa. The other potential reason could be the factor F_2 is under-predicted due to our assumptions and simplifications.

Fig. 13 gives the statistical comparison between simulated results and experiment data for KIMOF cases. The mean absolute percentage error (MAPE) and the mean relative percentage error (MRPE) are 78.6 % and 70.3 %, respectively, which are defined as:

$$\text{MAPE} = \frac{1}{n} \sum_{i=1}^{n} \frac{\left| \Delta T_{\text{sup},cal,i} - \Delta T_{\text{sup},exp} \right|}{\Delta T_{\text{sup},exp}} \times 100\% \tag{60}$$

$$\text{MRPE} = \frac{1}{n} \sum_{i=1}^{n} \frac{\Delta T_{\text{sup},cal,i} - \Delta T_{\text{sup},exp}}{\Delta T_{\text{sup},exp}} \times 100\% \tag{61}$$

It shows that in some cases there still exists large deviation in wall superheat temperature. Some data points are severely over-estimated by more than +50 %. Thus, as the first version at present stage, the new wall boiling heat transfer model still needs to be improved in further works. For example, the assumptions employed in the derivation and the coefficients simplified as constant can be meaningful subjects.

(a) IATF6 – IATF9

(b) IATF10 – IATF13
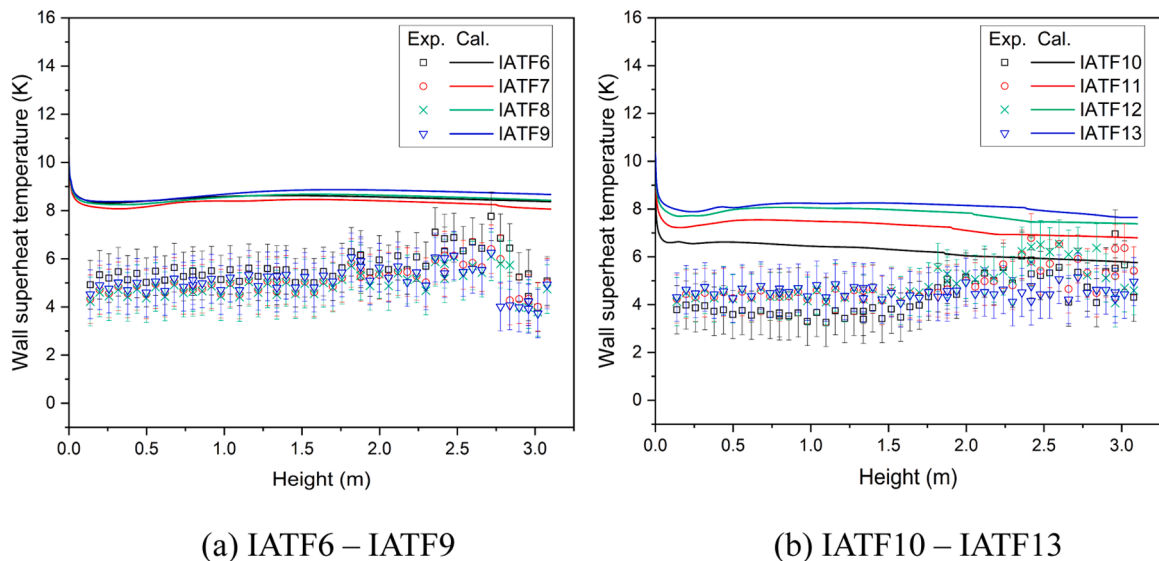
Fig. 11. Results of IATF experiments at 1.1 MPa.
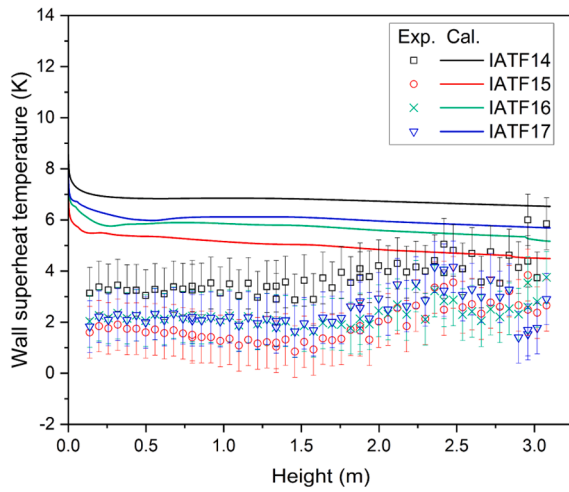
(a) IATF14 – IATF17
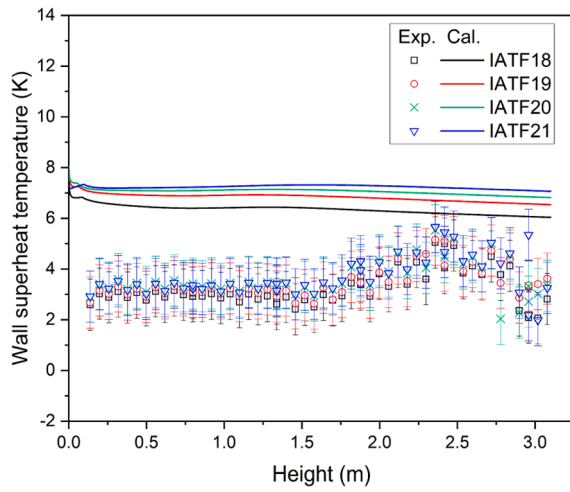
(b) IATF18 – IATF21

Fig. 12. Results of IATF experiments at 1.6 MPa.
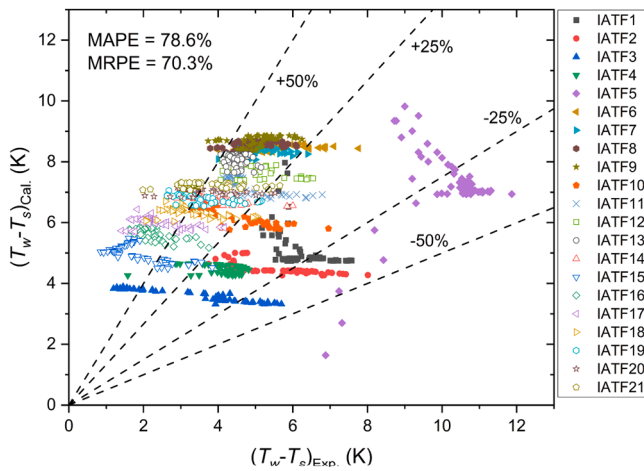
Fig. 13. Wall superheat temperature comparison between simulated and experimental results for KIMOF cases.

4. Sensitivity analysis

4.1. Mesh

According to the model derivation in Section 2.1, it can be speculated that the accuracy of the new model may be related to the mesh structure because of the implementation of void fraction in Eqs. (12) and (49), which is a local value in the first layer. Thus, four different meshes are tested and assessed based on the Bartolemei experiment in this part. The mesh information is given in Table 6. The Mesh1, Mesh2 and Mesh3 are uniformly divided with different number of nodes in the radial direction. To observe the effect of the first layer, Mesh4 has the same radial nodes with Mesh1, but controls the first layer thickness equaling to Mesh3 by

Table 6
Mesh information.

No.	Axial nodes	Radial nodes	First-layer thickness
Mesh1	1000	20	0.405 mm
Mesh2	1000	30	0.266 mm
Mesh3	1000	40	0.197 mm
Mesh4	1000	20	0.197 mm

non-uniform meshing. As shown in Fig. 14(a), the main influence region of mesh sizes on the wall temperature is the turning point that heat transfer capacity enhanced by boiling mechanism. It can be seen that as the radial nodes increases, the wall temperature decreases earlier. This is because that the increasing radial nodes means the first-layer thickness decreases, which will affect the value of local void fraction. On this basis, as presented in Fig. 14(b), the boiling correction factor (F_2) increases that enhancing the boiling heat transfer. So that the grid size could be an important point in the current model for wall temperature. In other word, the employment of the local void fraction in the first-layer in the new model should be improved in the future studies. Further, the comparison results of Mesh4 and Mesh3 show that the key point in mesh for the new model is the first-layer thickness. It is worth noting that the standard k-ε turbulence model and wall function request the wall Y-plus is larger than 30. Thus, Fig. 14(c) indicates the first-layer thickness cannot be further reduced for this experiment.

4.2. Coefficient C_1 in convective correction factor

As expounded in Section 2.2.2 pertaining to the convective correction factor, a coefficient C_1 is employed in Eq. (13) for the enhancement factor F_B, considering the boiling destructive effect of the thermal boundary layer. In prior preliminary validations, this coefficient was simply assigned a constant value of 10. However, it is imperative to acknowledge that the understanding of the boiling-induced deteriorative impact on the thermal boundary layer remains rudimentary within the existing physical model, necessitating further comprehensive investigation for the development of our new model. In this part, different values of C_1 have been used in the simulation of the Bartolemei experiment to study their impact on the predicted results. The results, depicted in Fig. 15, demonstrate that variations in C_1 within the range of 5–30 has minimal influence on both wall temperature and the cross-section average liquid temperature, particularly in the domain of single-phase convection and the initial boiling regime (where height < 0.75 m). This phenomenon can be attributed to the negligible impact of attached bubbles on convective heat transfer when vapor concentrations are small, as corroborated by Fig. 15(c), which illustrates that the convective correction factor closely approximates 1 in these regions. Conversely, the value of C_1 exerts a more substantial influence on the void fraction, particularly the void fraction within the first layer. As evidenced by Fig. 15(b), variations in C_1 result in divergent heat flux partitioning. Specifically, a larger value of C_1 corresponds to a larger contribution of convective heat transfer, consequently yielding lower
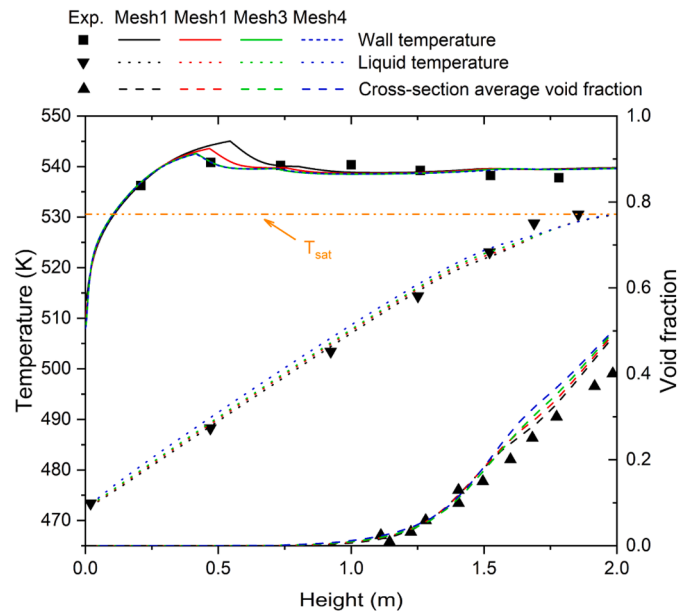
(a) Wall temperature, liquid temperature and void fraction
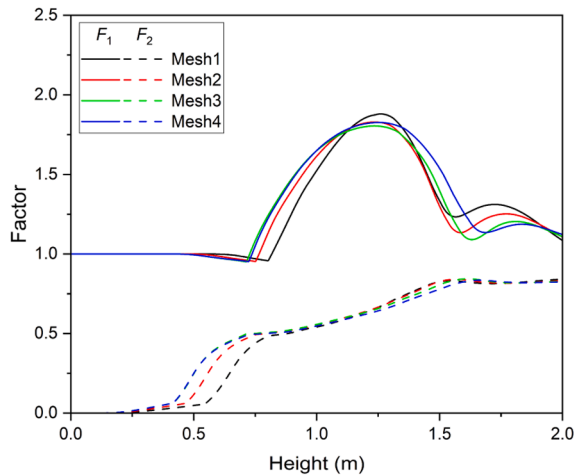
(b) Correction factors
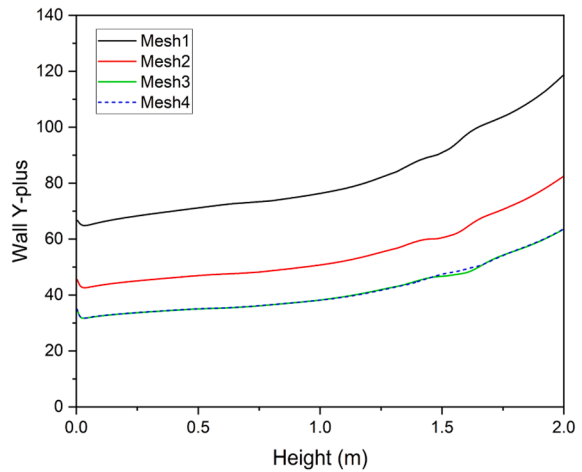
(c) Wall Y-plus

Fig. 14. Sensitivity analysis of mesh.

void fraction within the first-layer of grids and lower cross-section averaged void fraction.

4.3. Coefficient C_2 in boiling correction factor

Fig. 16 presents the results obtained through varying the coefficient C_2, an integral component in the boiling correction factor, as discussed in Section 2.2.2. The most pronounced distinctions emerge in the initial stages of boiling, wherein the boiling heat transfer mechanism commences to exert influence. Consequently, the positive slope of wall temperature diminishes and even transition to a negative slope during this phase. As the value of C_2 increases, the predicted wall temperature concurrently rises. This phenomenon is attributed to the relationship delineated in Eq. (57), where an increased coefficient C_2 corresponds to a reduced value of the boiling correction factor, as depicted in Fig. 16(b). This reduction, in turn, leads to a reduced contribution of boiling heat transfer to the overall heat flux. However, the predicted cross-section average liquid temperature and void fraction exhibit minimal fluctuations within the C_2 range of 0.1 to 1.5, because there is little vapor

generated in cross-section at the beginning of boiling and also little interfacial heat transfer in bulk flow.

5. Conclusions

In this study, a new semi-mechanistic wall boiling heat transfer model was developed for CFD applications. The new model partitioned the wall heat flux into two parts: the convective heat flux and the nucleate boiling heat flux. Two correction factors were deduced based on the analysis of bubble growth mechanism. As a final expression, the new model was given by:
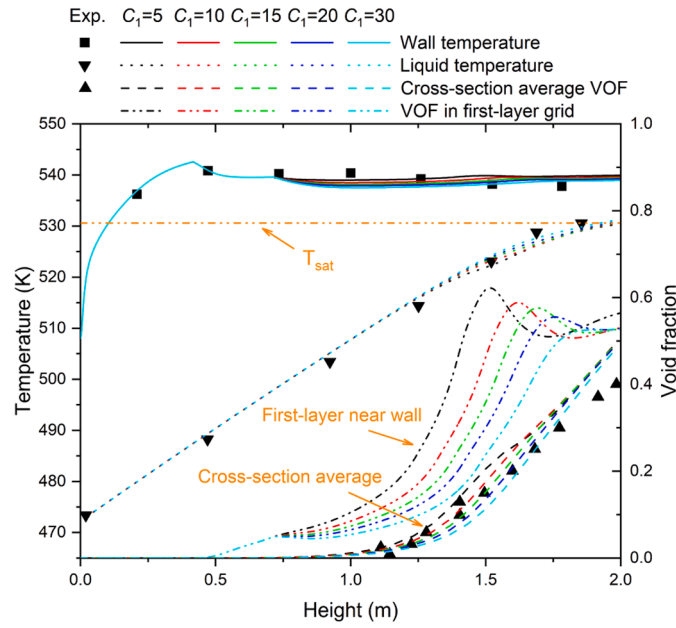
(a) Wall temperature, liquid temperature and void fraction
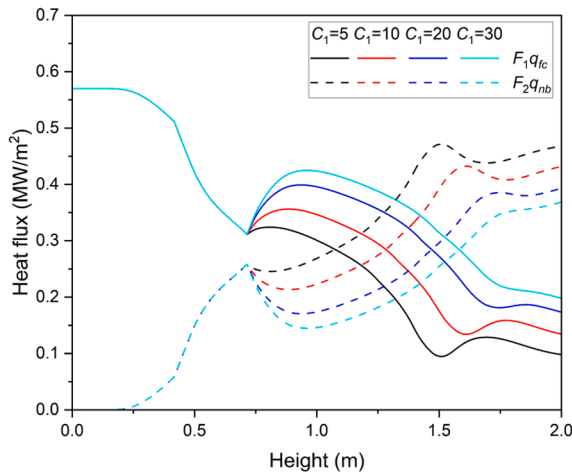
(b) Wall heat flux partitioning
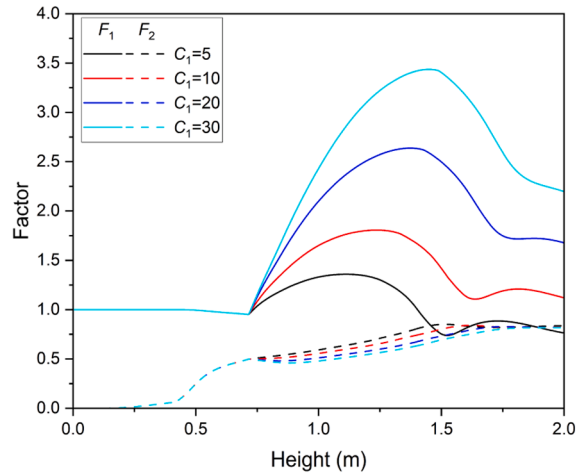
(c) Correction factors

Fig. 15. Sensitivity analysis of coefficient C1.

$$q_w = F_1 \cdot q_{fc} + F_2 \cdot q_{nb}$$

$$
\begin{cases}
q_{fc} - \text{Wall function approach in CFD} \\[2mm]
q_{nb} = 0.00122 \dfrac{\lambda_l^{0.79} C_{p,l}^{0.45} \rho_l^{0.49}}{\sigma^{0.5} \mu_l^{0.29} h_{lg}^{0.24} \rho_g^{0.24}} (T_w - T_s)^{0.24} (P_w - P_s)^{0.75} \cdot (T_w - T_s) \\[3mm]
F_1 = (1 - \alpha_g) \cdot \left(1 + C_1 \dfrac{q_E}{h_{fg} \rho_v} \sqrt{\dfrac{\rho_l}{\tau_w}} \right) \\[3mm]
F_2 = \dfrac{1}{1 + \left(\sqrt{2} \cdot C_2 \cdot \frac{1 - \alpha_g}{\alpha_g} \cdot \frac{B_{LB}}{B_{WB}^2 \cdot B_{WB}} \cdot \frac{\rho_v h_{fg}}{\rho_l C_{P,l}} \right)^{0.5} \cdot \left(\frac{1}{T_w - T_s} \right)^{0.5}}
\end{cases}
\tag{62}
$$

One of the key features is the new wall boiling heat transfer model was proposed for CFD methodology. This model computes each parameter based on local physical properties and macroscopic parameters at the cell level, while without the necessity of bulk flow parameters or micro-parameters. The results obtained through various validation tests indicated that the new model could predict reasonable wall temperature against the experimental data. The new model offers a new approach to treat the wall boiling heat transfer and to be easily adopted in CFD simulations. However, the analysis and simulation results also revealed some limitations of the new model and indicated a scope for the further development:

(a) A comprehensive analysis of the basic assumption ($Q_{WB} = Q_{WB,P}$) or a new relationship between both heat transfers is required.

(b) The calculation of the boiling heat transfer coefficient is currently based on the Forster-Zuber model [33], necessitating experimentation with different correlations under varying conditions.
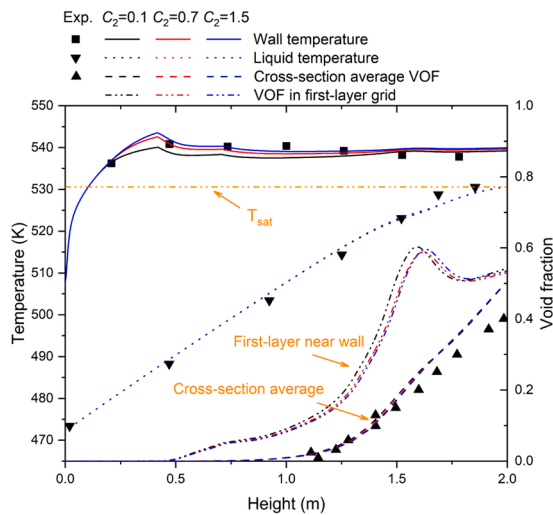
(a) Wall temperature, liquid temperature and void fraction
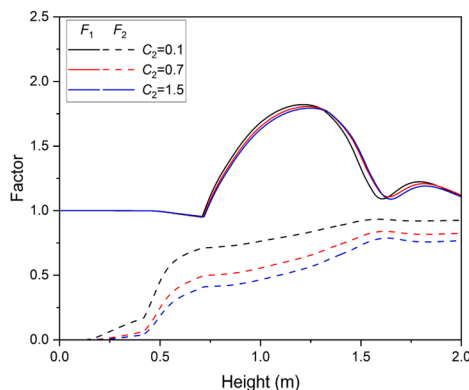
(b) Correction factors

Fig. 16. Sensitivity analysis of coefficient C2.

(c) A simple linear function was taken to account the effect of bubble growth on the convective heat transfer. Further investigations are required.

(d) To separately consider the bubble influenced area and liquid covered region, the void fraction in the first-layer cell is introduced, which depends on local value that related to the grid size.

(e) The coefficients (C_1 and C_2) introduced in the new model as constants need further investigation and improvement, if necessary.

CRediT authorship contribution statement

Xiang Zhang: Data curation, Investigation, Software, Validation, Writing – original draft. **Xu Cheng:** Conceptualization, Methodology, Project administration, Writing – review & editing. **Wei Liu:** Methodology, Writing – review & editing.

Declaration of competing interest

The authors declare that they have no known competing financial interests or personal relationships that could have appeared to influence the work reported in this paper.

Data availability

Data will be made available on request.

Acknowledgements

References

[1] N. Basu, G.R. Warrier, V.K. Dhir, Wall heat flux partitioning during subcooled flow boiling: part 1–model development, J. Heat Transf. 127 (2) (2005) 131–140.

[2] W.H. McAdams, W.E. Kennel, C.S. Minden, R. Carl, P.M. Picornell, J.E. Dew, Heat transfer at high rates to water with surface boiling, Ind. Eng. Chem. 41 (9) (1949) 1945–1953.

[3] J.R.S. Thorn, W.M. Walker, T.A. Fallon, G.F.S. Reising, Paper 6: boiling in sub-cooled water during flow up heated tubes or annuli, in: Proceedings of the Institution of Mechanical Engineers, Conference Proceedings 180, 1965, pp. 226–246.

[4] S. Kandlikar, Heat transfer characteristics in partial boiling, fully developed boiling, and significant void flow regions of subcooled flow boiling, J. Heat Transf. Trans. ASME 120 (1998) 395–401.

[5] X. Fang, Y. Yuan, A. Xu, L. Tian, Q. Wu, Review of correlations for subcooled flow boiling heat transfer and assessment of their applicability to water, Fusion Eng. Des. 122 (2017) 52–63.

[6] M.M. Mahmoud, T.G. Karayiannis, Heat transfer correlation for flow boiling in small to micro tubes, Int. J. Heat Mass Transf. 66 (2013) 553–574.

[7] N. Kurul, M.Z. Podowski, On the modeling of multidimensional effects in boiling channels, in: Proceedings of the 27th National Heat Transfer Conference, Minneapolis, Minn, USA, ASME, 1991.

[8] E. Krepper, B. Končar, Y. Egorov, CFD modelling of subcooled boiling - concept, validation and application to fuel assembly design, Nucl. Eng. Des. 237 (7) (2007) 716–731.

[9] X. Zhang, R. Li, M. Peng, T. Cong, C. He, G. Xia, X. Wei, Numerical analysis on subcooled boiling in PWR coolant channel based on a modified multi-scale interface model, Appl. Therm. Eng. 229 (2023) 120598.

[10] K. Liu, M. Wang, F. Gan, W. Tian, S. Qiu, G.H. Su, Numerical investigation of flow and heat transfer characteristics in plate-type fuel channels of IAEA MTR based on OpenFOAM, Prog. Nucl. Energy 141 (2021) 103963.

[11] J. Shi, R. Zhang, Z. Zhu, T. Ren, C. Yan, A modified wall boiling model considering sliding bubbles based on the RPI wall boiling model, Int. J. Heat Mass Transf. 154 (2020) 119776.

[12] M. Wang, L. Li, K. Liu, J. Zhang, W. Tian, S. Qiu, G. Su, Development of subcooled wall boiling model considering bubble sliding in narrow rectangular channel, Int. J. Therm. Sci. 181 (2022) 107787.

[13] S.C.P. Cheung, S. Vahaji, G.H. Yeoh, J.Y. Tu, Modeling subcooled flow boiling in vertical channels at low pressures–Part 1: assessment of empirical correlations, Int. J. Heat Mass Transf. 75 (2014) 736–753.

[14] J. Gu, Q. Wang, Y. Wu, J. Lyu, S. Li, W. Yao, Modeling of subcooled boiling by extending the RPI wall boiling model to ultra-high pressure conditions, Appl. Therm. Eng. 124 (2017) 571–584.

[15] Y.C. Lin, Y. Zhao, M. Ishii, J.P. Schlegel, K.J. Hogan, J.R. Buchanan, Assessment of nucleation boiling models and improvement by the chen correlation for two-fluid model CFD, Int. J. Heat Mass Transf. 175 (2021) 121363.

[16] J.F. Klausner, R. Mei, D.M. Bernhard, Vapor bubble departure in forced convection boiling, Int. J. Heat Mass Transf. 36 (3) (1993) 651–662.

[17] M. Colombo, M. Fairweather, Prediction of bubble departure in forced convection boiling: a mechanistic model, Int. J. Heat Mass Transf. 85 (2015) 135–146.

[18] J.Y. Tu, G.H. Yeoh, On numerical modelling of low-pressure subcooled boiling flows, Int. J. Heat Mass Transf. 45 (6) (2002) 1197–1209.

[19] Y. Zhang, R. Zhang, W. Tian, G.H. Su, S. Qiu, Numerical prediction of CHF based on CFD methodology under atmospheric pressure and low flow rate, Appl. Therm. Eng. 149 (2019) 881–888.

[20] J.C. Chen, Correlation for boiling heat transfer to saturated fluids in convective flow, Ind. Eng. Chem. Process Des. Dev. 5 (1966) 322–329.

[21] N.I. Kolev, Multiphase Flow Dynamics 2: Thermal and Mechanical Interactions, Springer, Germany, 2007 (v. 2).

[22] A. Feldman, C. Marvillet, M. Lebouché, Nucleate and convective boiling in plate fin heat exchangers, Int. J. Heat Mass Transf. 43 (18) (2000) 3433–3442.

[23] W. Qu, I. Mudawar, Flow boiling heat transfer in two-phase micro-channel heat sinks–I. Experimental investigation and assessment of correlation methods, Int. J. Heat Mass Transf. 46 (2003) 2755–2771.

[24] G. Orian, M. Jelinek, A. Levy, Flow boiling of binary solution in horizontal tube, Energy 35 (1) (2010) 35–44.

[25] D. Liu, S.V. Garimella, Flow boiling heat transfer in microchannels, J. Heat Transf. 129 (10) (2007) 1321–1332.

[26] J. Yan, Q. Bi, Z. Liu, G. Zhu, L. Cai, Subcooled flow boiling heat transfer of water in a circular tube under high heat fluxes and high mass fluxes, Fusion Eng. Des. 100 (2015) 406–418.

[27] H. Steiner, A. Kobor, L. Gebhard, A wall heat transfer model for subcooled boiling flow, Int. J. Heat Mass Transf. 48 (19–20) (2005) 4161–4173.

[28] M. Sonntag, Subcooled Two-Phase Flow Heat Transfer in Multiscale Systems, Karlsruhe Institute of Technology, Germany, 2017.

[29] C. Paz, E. Suárez, M. Concheiro, A. Copo, V. Tobio, CFD implementation and experimental validation of the Chen model for heat transfer in nucleate boiling. Computational Methods in Multiphase Flow VII, WIT Press, 2013, pp. 377–385.

[30] S. Das, H. Punekar, On development of a semimechanistic wall boiling model, J. Heat Transf. 138 (6) (2016) 061501.

[31] ANSYS-Fluent, ANSYS Fluent Theory Guide, ANSYS Inc., USA, 2020.

[32] C. Jayatillaka, The influence of prandtl number and surface roughness on the resistance of the laminar sublayer to momentum and heat transfer, Prog. Heat Mass Transf. 1 (1969) 193–321.

[33] H.K. Forster, N. Zuber, Dynamics of vapor bubbles and boiling heat transfer, AIChE J. 1 (4) (1955) 531–535.

[34] A.A. Abed, A. Bonanos, F. Moukalled, Numerical simulation of flow boiling heat transfer and pressure drop in a corrugated plate heat exchanger at low mass flux and vapor quality conditions, Numer. Heat Transf. Part A Appl. 80 (11) (2021) 556–578.

[35] Z. Chen, W. Li, J. Li, K. Zhou, Z. Feng, A new correlation for subcooled flow boiling heat transfer in a vertical narrow microchannel, J. Electron. Packag. 143 (1) (2021) 014501.

[36] M.G. Cooper, The microlayer and bubble growth in nucleate pool boiling, Int. J. Heat Mass Transf. 12 (8) (1969) 915–933.

[37] F. Demiray, J. Kim, Microscale heat transfer measurements during pool boiling of FC-72: effect of subcooling, Int. J. Heat Mass Transf. 47 (14–16) (2004) 3257–3268.

[38] S. Jung, H. Kim, An experimental method to simultaneously measure the dynamics and heat transfer associated with a single bubble during nucleate boiling on a horizontal surface, Int. J. Heat Mass Transf. 73 (2014) 365–375.

[39] Y. Utaka, Y. Kashiwabara, M. Ozaki, Z. Chen, Heat transfer characteristics based on microlayer structure in nucleate pool boiling for water and ethanol, Int. J. Heat Mass Transf. 68 (2014) 479–488.

[40] R. Zhang, T. Cong, W. Tian, S. Qiu, G. Su, Effects of turbulence models on forced convection subcooled boiling in vertical pipe, Ann. Nucl. Energy 80 (2015) 293–302.

[41] Y. Sato, K. Sekoguchi, Liquid velocity distribution in two-phase bubble flow, Int. J. Multiph. Flow 2 (1) (1975) 79–95.

[42] M. Ishii, Two-fluid model for two-phase flow, Multiph. Sci. Technol. 5 (1–4) (1990) 1–63.

[43] F.J. Moraga, F.J. Bonetto, R.T. Lahey, Lateral forces on spheres in turbulent uniform shear flow, Int. J. Multiph. Flow 25 (6–7) (1999) 1321–1372.

[44] M.A.L. De Bertodano, Turbulent Bubbly Two-Phase Flow in a Triangular Duct, Rensselaer Polytechnic Institute, Troy, New York, USA, 1992.

[45] W. Ranz, W. Marshall, Evaporation from drops, Chem. Eng. Prog. 48 (3) (1952) 141–146.

[46] J. Laviéville, E. Quemerais, S. Mimouni, M. Boucker, N. Mechitoua, NEPTUNE CFD V1.0 theory manual, EDF, France, 2005.

[47] G.G. Bartolemei, V.M. Chanturiya, Experimental study of true void fraction when boiling subcooled water in vertical tubes, Therm. Eng. 14 (2) (1967) 123–128.

[48] J. Garnier, E. Manon, G. Cubizolles, Local measurements on flow boiling of refrigerant 12 in a vertical tube, Multiph. Sci. Technol. 13 (2001) 1–111.

[49] L. Köckert, A.F. Badea, X. Cheng, D. Yu, D. Klingel, Studies on post-dryout heat transfer in R-134a vertical flow, Int. J. Adv. Nucl. React. Des.Technol. 3 (2021) 44–53.